International Journal of Refrigeration 139 (2022) 180–191

Contents lists available at ScienceDirect

International Journal of Refrigeration

journal homepage: www.elsevier.com/locate/ijrefrig

Efficient modeling of adsorption chillers: Avoiding discretization by operator splitting

Modélisation efficace des refroidisseurs à adsorption : éviter la discrétisation par le fractionnement des opérateurs

Andrej Gibelhaus [a], Patrik Postweiler [a], André Bardow [*,a,b,c]

[a] *Institute of Technical Thermodynamics, RWTH Aachen University, 52062 Aachen, Germany*
[b] *Institute of Energy and Climate Research - Energy Systems Engineering (IEK-10), Jülich Research Center, 52425 Jülich, Germany*
[c] *Institute of Energy and Process Engineering, Energy and Process Systems Engineering, ETH Zurich, 8092 Zurich, Switzerland*

ARTICLE INFO

Keywords:
Lumped-parameter model
Plug-flow
Computational efficiency
Experimental validation
Silica gel - water adsorption chiller

Mots clés:
Modèle à paramètres localisés
Écoulement à bouchons
Efficacité de calcul
Validation expérimentale
Refroidisseur à adsorption de gel de silice-eau

ABSTRACT

Reliable and computationally efficient models are crucial to improve the performance of adsorption chillers. However, modeling of adsorption chillers is challenging due to the intrinsic process dynamics. Currently, adsorption chillers are most often represented by 1-d, lumped-parameter models that use lumped models for all components but resolve the heat exchangers in one spatial dimension. Still, accurate simulations require fine discretization leading to poor computational efficiency. To increase computational efficiency, here, an alternative modeling approach is proposed that avoids discretization by applying operator splitting.

The benefits of the proposed modeling approach are demonstrated in two real-world case studies. First, the resulting adsorption chiller model is calibrated and validated with experimental data of a lab-scale one-bed adsorption chiller: The proposed model retains the accuracy of a state-of-the-art model while increasing computational efficiency by up to 70%. Second, the proposed model is applied to a commercial two-bed adsorption chiller with excellent accuracy. Finally, the validity of model is tested by varying the ratio between the overall heat transfer coefficient and the heat capacity rate of the fluid in the heat exchangers. The proposed model is shown to be well suited for the conditions present in most adsorption chillers.

Notation

Latin symbols		
A	area	m^2
A	adsorption potential	J/kg
$A(W)$	adsorption potential as function of filled pore volume	J/kg
c	specific heat capacity	J/(kgK)
D	diffusion coefficient	m^2/s
h	specific enthalpy	J/kg
h	heat transfer coefficient	$W/(m^2K)$
m	mass	kg
$\dot{m}$	mass flow	kg/s
p	pressure	P a
Q	thermal energy	J
$\dot{Q}$	heat flow	W
r	radius	m

(*continued on next column*)

(*continued*)

R	universal gas constant	J/(kgK)
t	time	s
T	temperature	°C or K
u	specific internal energy	J/kg
U	overall heat transfer coefficient	$W/(m^2K)$
v	velocity	m/s
V	volume	m^3
w	loading	kg/kg
W	filled pore volume	m^3/kg
x	axial coordinate	m
Greek symbols		
Δ	difference	
δ	infinitesimal difference	
ρ	density	kg/m^3
Subscripts and superscripts		

(*continued on next page*)

* Corresponding author.
E-mail address: abardow@ethz.ch (A. Bardow).

https://doi.org/10.1016/j.ijrefrig.2022.04.015
Received 14 May 2021; Received in revised form 11 April 2022; Accepted 12 April 2022
Available online 15 April 2022

(*continued*)

A	adsorber
ad	adsorbed phase
ads	adsorption
bed	adsorber bed
C	condenser
conv	convective
E	evaporator
eff	effective
eq	equivalent
ext	external
fl	heat exchanger fluid
flow	fluid flow
in	inlet
int	internal
liq	liquid
meas	measured
out	outlet
port	fluid port
sat	saturated
sim	simulated
sor	adsorbent
v	vapor phase
v	at constant volume
Abbreviations and Acronyms	
COP	coefficient of performance (J/J)
CV	coefficient of variation
CN	characteristic number
disc	discretized
HX	heat exchanger
LDF	linear driving force
PF	plug-flow
RMSD	root-mean-square deviation
SCP	specific cooling power (W/kg)
VLE	vapor-liquid equilibrium

1. Introduction

Adsorption chillers can provide sustainable cooling by employing environmentally friendly working pairs and heat as driving energy (Denzinger et al., 2021). Modeling of adsorption chillers is key for design and optimization (Yong and Sumathy, 2002). However, modeling of adsorption chillers is challenging, due to its intrinsic dynamic nature and the impact of several interacting components on performance (Gibelhaus et al., 2019). Due to this complexity, system-level studies often use grey- or black-box models, e.g., based on performance maps (Buonomano et al., 2018; Palomba et al., 2018), polynomial regression analysis (Sawant et al., 2020), or artificial neural networks (Krzywanski et al., 2017; Lazrak et al., 2016). Although grey- and black-box models are computationally very efficient, these models do not deliver insights into the adsorption chiller process to improve the adsorption chiller itself. Physics-based models are therefore required.

However, a detailed consideration of all physical effects results in a high computational effort, inappropriate for system-level optimization (Pesaran et al., 2016). Thus, a trade-off is observed between model accuracy and computational efficiency. Several literature reviews (Pesaran et al., 2016; Sah et al., 2017; Teng et al., 2016; Yong and Sumathy, 2002) classify adsorption chiller models into three main classes with an increasing level of complexity: (1) thermodynamic equilibrium models, (2) lumped-parameter models, and (3) distributed-parameter models (heat and mass transfer models):

(1) Thermodynamic equilibrium models are based on a steady-state analysis of the first- and second-law of the adsorption chiller cycle. Thus, this model class is particularly useful to evaluate and compare the potential of different cycles (Alam et al., 2004), working pairs (Calabrese et al., 2020), and applications (Meunier et al., 1998; Sha and Baiju, 2021). However, thermodynamic equilibrium models neglect adsorption kinetics. Therefore, this model class cannot predict the performance of real adsorption chillers.

(2) Lumped-parameter models employ transient mass and energy balances combined with overall, effective transport resistances to consider adsorption kinetics (dynamic models). Already in early pioneering studies, Saha et al. (1995) developed and experimentally validated (Boelman et al., 1995) a lumped-parameter model of a two-bed adsorption chiller to investigate the influence of operating conditions on the performance. Also today, this model class is widely used to estimate the performance of adsorption chillers for different control strategies (Gråber et al., 2011; Muttakin et al., 2020), operating conditions (Tso et al., 2012), working pairs (Graf et al., 2019), and component designs (Abd-Elhady and Hamed, 2020; Sharafian and Bahrami, 2015). The main drawback of lumped-parameter models is that they cannot capture the specific geometries of the components and the fast dynamics of the heat transfer fluid, as the spatial resolution is neglected.

(3) The next level of detail is provided by distributed-parameter models, which resolve the states in a component in time and space (Pesaran et al., 2016). Thus, this model class is usually employed for detailed investigations of the adsorption process (Dawoud et al., 2007), the adsorbent configuration (Radu et al., 2017), and the heat exchanger design (Mahdavikhah and Niazmand, 2013). However, the simulation of an adsorption chiller can take several hours (Graf et al., 2020; Yaïci and Entchev, 2019). Consequently, the computational efficiency is usually too poor for system-level optimizations.

Lumped-parameter models are currently most suitable and popular for system-level applications, due to a good compromise between accuracy and computational efficiency (Mohammed et al., 2019). However, lumped-parameter models are not able to capture the fast dynamics of the heat transfer fluid (Douss et al., 1988; Karagiorgas and Meunier, 1987) and, therefore, show deviations between simulations and measurements (Dalibard, 2017; Schicktanz and Núñez, 2009; Wu et al., 2000). Thus, lumped-parameter models were refined by heat exchangers discretized in one dimension (1-d) (Critoph, 1999). These 1-d, lumped-parameter models significantly improve accuracy compared to the original lumped-parameter models, while still providing a much higher computational efficiency than distributed-parameter models (Wang and Chua, 2007).

However, 1-d, lumped-parameter models still lead to a trade-off between accuracy and computational efficiency: Accurate results require a fine discretization of the adsorber heat exchanger (Lanzerath, 2013), which, in turn, decreases the computational efficiency. As high computational efficiency is crucial for system-level optimizations (Nienborg et al., 2017) and real-time applications (Bau et al., 2019), the discretization resolution is usually reduced at the cost of accuracy.

In this work, we propose a modeling alternative for adsorption chillers that resolves the trade-off between accuracy and computational efficiency of 1-d, lumped-parameter models. The discretization of the heat exchangers is avoided by applying operator splitting to the convective transport equation (van der Heijde et al., 2017). Operator splitting allows for an analytical solution of the transport equation, instead of numerical discretization. Thereby, the computational efficiency of the heat exchanger models can be significantly improved while maintaining a high accuracy.

This paper is structured as follows: In Section 2.1, we introduce the proposed model. In Section 3 the proposed model is compared with experimental data from a lab-scale one-bed adsorption chiller and a 1-d, lumped-parameter model. In Section 4, we validate the proposed model for a commercial two-bed adsorption chiller. In Section 5, we investigate the validity range of the proposed modeling approach. In Section 6 the main results are summarized.

2. Modeling

In this section, the model of the adsorption chiller is briefly introduced. For more details about the model the reader is referred to the supporting information A.

The adsorption chiller model has three main components: Adsorber, evaporator, and condenser. Each component consists of sub-models for the heat exchanger and the adsorber bed or the vapor liquid equilibrium (VLE). These sub-models are presented in the following.

2.1. Plug-flow-based heat exchanger

The proposed heat exchanger model eliminates the discretization and thereby resolves the trade-off between accuracy and computational efficiency of 1-d, lumped-parameter models. Instead of discretizing the convective term the proposed approach applies operator splitting to the transport equation of the heat transfer fluid. Operator splitting allows for an efficient, analytical solution of the convective heat transfer.

The heat exchanger is a key component of the adsorption chiller. An accurate representation of the heat exchanger typically requires a model with spatial discretization in one dimension, cf. Section 1. Here, we avoid the spatial discretization by a plug-flow-based approach. The plug-flow-based approach is inspired by the thermo-hydraulic pipe model proposed by van der Heijde et al. (2017) to describe pipes in heating networks. Here, the thermo-hydraulic pipe model is adapted for adsorption chillers to describe the heat transfer between the heat transfer fluid and the thermally connected models, i.e., the adsorber bed and the VLE volume.

Since liquid water is used as heat transfer fluid in the heat exchangers, the flow in the heat exchanger can be described as incompressible, 1-d convective flow (Batchelor, 2000). Thus, the mass balance for each sub-model results from the continuity equation as:

$$\dot{m}_{\mathrm{fl,in}} - \dot{m}_{\mathrm{fl,out}} = 0, \tag{1}$$

where $\dot{m}_{\mathrm{fl,in}}$ is the entering and $\dot{m}_{\mathrm{fl,out}}$ is the leaving mass flow. Neglecting axial diffusion and internal sources due to dissipation (Roetzel et al., 2020), the energy balances of the fluid and the heat exchanger wall read:

$$m_{\mathrm{fl}} \frac{\partial h_{\mathrm{fl}}}{\partial t} + m_{\mathrm{fl}} v_{\mathrm{fl}} \frac{\partial h_{\mathrm{fl}}}{\partial x} = -h_{\mathrm{ext}} A_{\mathrm{ext}} \left(T_{\mathrm{fl}} - T_{\mathrm{wall}}\right) \tag{2}$$

$$m_{\mathrm{wall}} c_{\mathrm{wall}} \frac{\partial T_{\mathrm{wall}}}{\partial t} = h_{\mathrm{ext}} A_{\mathrm{ext}} \left(T_{\mathrm{fl}} - T_{\mathrm{wall}}\right) - h_{\mathrm{int}} A_{\mathrm{int}} \left(T_{\mathrm{wall}} - T_{\mathrm{process}}\right), \tag{3}$$

where m_{fl} is the mass, h_{fl} is the specific enthalpy, v_{fl} is the velocity, and T_{fl} is the temperature of the fluid. The mass, the specific heat capacity, and the temperature of the heat exchanger wall are given by m_{wall}, c_{wall}, and T_{wall}, respectively. The independent variables are the time t and the axial coordinate x. To describe the heat transfer, the heat transfer value of the external heat transfer fluid[1] $h_{\mathrm{ext}}A_{\mathrm{ext}}$ and the heat transfer value of the internal process side, e.g. the adsorbent or VLE volume, $h_{\mathrm{int}}A_{\mathrm{int}}$ are used. The temperature T_{process} is the process-side temperature of the heat exchanger, i.e., the adsorbent in the adsorber and the VLE volume in the evaporator and condenser.

To solve Equations (2) and (3), the classical finite-volume approach approximates the spatial derivative $\left(\frac{\partial h_{\mathrm{fl}}}{\partial x}\right)$ by spatial discretization using a backward difference (upwind) scheme (Roetzel et al., 2020). The spatial discretization leads to an ordinary differential equations system, which can be large and computationally expensive for a fine discretization.

Instead of spatial discretization, the plug-flow-based approach applies some simplifications: First, we neglect the thermal mass of the heat exchanger wall for the dynamics and consider the wall in steady-state ($m_{\mathrm{wall}} c_{\mathrm{wall}} \frac{\partial T_{\mathrm{wall}}}{\partial t} \approx 0$ in Equation 3). For adsorption chillers, the dynamics of the heat exchanger wall are usually much faster than the dynamics of the adsorber bed, since the heat transfer to the heat exchanger wall is much better than to the adsorbent. Thus, the dynamics of the heat exchanger wall can be neglected. In contrast to the dynamics, the thermal energy needed to heat up and cool down the heat exchanger wall substantially influences the performance of adsorption chillers (Gluesenkamp et al., 2020) and, thus, has to be considered. We consider this thermal energy by adding an energetically equivalent fluid volume after the calculation of the heat transfer as discussed below. Due to the neglected dynamics of the heat exchanger wall, Equations (2) and (3) simplify to:

$$m_{\mathrm{fl}} \frac{\partial h_{\mathrm{fl}}}{\partial t} + m_{\mathrm{fl}} v_{\mathrm{fl}} \frac{\partial h_{\mathrm{fl}}}{\partial x} = -U_{\mathrm{ext}} A_{\mathrm{ext}} \left(T_{\mathrm{fl}} - T_{\mathrm{process}}\right) \tag{4}$$

with the overall heat transfer value through the wall $U_{\mathrm{ext}}A_{\mathrm{ext}}$:

$$U_{\mathrm{ext}} A_{\mathrm{ext}} = \frac{h_{\mathrm{ext}} A_{\mathrm{ext}} \cdot h_{\mathrm{int}} A_{\mathrm{int}}}{h_{\mathrm{ext}} A_{\mathrm{ext}} + h_{\mathrm{int}} A_{\mathrm{int}}}. \tag{5}$$

Second, we apply operator splitting (MacNamara and Strang, 2016) to Equation 4. Thereby, the total specific enthalpy change of the fluid over the heat exchanger Δh_{fl} (Equation 4) is split into 1) the specific enthalpy change due to the enthalpy flow of the fluid $\Delta h_{\mathrm{fl}}^{\mathrm{flow}}$ and 2) the specific enthalpy change due to the convective heat transfer from or to the fluid $\Delta h_{\mathrm{fl}}^{\mathrm{conv}}$:

$$\Delta h_{\mathrm{fl}} = \Delta h_{\mathrm{fl}}^{\mathrm{flow}} + \Delta h_{\mathrm{fl}}^{\mathrm{conv}}. \tag{6}$$

Both specific enthalpy changes are calculated sequentially.

Enthalpy flow of the fluid

The enthalpy flow of the fluid (Equation 7) describes the energy transport through the heat exchanger due to the fluid flow but without considering the convective heat transfer from or to the fluid:

$$\frac{\partial h_{\mathrm{fl}}^{\mathrm{flow}}}{\partial t} + v_{\mathrm{fl}} \frac{\partial h_{\mathrm{fl}}^{\mathrm{flow}}}{\partial x} = 0. \tag{7}$$

Equation 7 considers the dynamics of the fluid flow before calculating the heat transfer in the next step (Equation 8). Thus, the model first considers the time needed by the heat transfer fluid to flow through the heat exchanger. This time delays the heat transfer. The time delay is particularly important during the switches between adsorption and desorption phase (and vice versa). Without the time delay, any change in the inlet temperature would immediately change the temperature throughout the heat exchanger and thereby change the heat transfer according to steady-state calculation. In reality, the heat transfer fluid needs to flow through the heat exchanger before contributing to the heat transfer.

Equation 7 is efficiently solved by the Modelica operator *spatialDistribution()*, which keeps track of the spatial distribution of the transported property (in this case the specific enthalpy), by suitable sampling, interpolation, and shifting the stored distribution. For more details about the implementation of the operator, the reader is referred to the language specifications of Modelica (Modelica Association, 2017).

Convective heat transfer

The convective heat transfer (Equation 8) describes the energy transport between the fluid and the process-side of the adsorption chiller. To compute this heat transfer, the Lagrangian approach is used to allow for an analytical solution of the outlet temperature of the fluid (van der Heijde et al., 2017; Oppelt et al., 2016): The Lagrangian

[1] In the following, the product of the heat transfer coefficient h and the heat transfer area A is referred to as heat transfer value hA to avoid long expressions.

approach attaches the coordinate system to a moving fluid particle flowing through the heat exchanger. Due to the attached coordinate system, there is no spatial distribution in the energy balance of a moving fluid particle of infinitesimal length δx:

$$m_{\mathrm{fl}} \frac{dh_{\mathrm{fl}}^{\mathrm{conv}}}{dt} \delta x = -U_{\mathrm{ext}} A_{\mathrm{ext}} \left(T_{\mathrm{fl}}^{\mathrm{conv}} - T_{\mathrm{process}} \right) \delta x. \tag{8}$$

Expressing the specific enthalpy change by the temperature change and rearranging Equation 8 leads to:

$$\int_{T_{\mathrm{fl,in}}^{\mathrm{conv}}}^{T_{\mathrm{fl,out}}^{\mathrm{conv}}} \frac{m_{\mathrm{fl}} c_{\mathrm{fl}}}{U_{\mathrm{ext}} A_{\mathrm{ext}}} \frac{\mathrm{d}T_{\mathrm{fl}}^{\mathrm{conv}}}{T_{\mathrm{fl}}^{\mathrm{conv}} - T_{\mathrm{process}}} = - \int_{t_{\mathrm{in}}}^{t_{\mathrm{out}}} \mathrm{d}t. \tag{9}$$

The integral on the left of Equation 9 can be solved analytically under the following assumptions:

1. The temperature dependency of both, the overall heat transfer coefficient U_{ext} and the fluid properties (ρ_{fl} and c_{fl}) is negligible within the integration range ($T_{\mathrm{fl,in}}^{\mathrm{conv}}$ and $T_{\mathrm{fl,out}}^{\mathrm{conv}}$).
2. Each entering fluid particle is exposed to a constant temperature T_{process} while flowing through the heat exchanger.

With these assumptions, Equation 10 delivers the analytical solution for the outlet temperature $T_{\mathrm{fl,out}}^{\mathrm{conv}}$:

$$T_{\mathrm{fl,out}}^{\mathrm{conv}}(t_{\mathrm{out}}) = T_{\mathrm{process}}(t_{\mathrm{in}}) + \left(T_{\mathrm{fl,in}}^{\mathrm{conv}}(t_{\mathrm{in}}) - T_{\mathrm{process}}(t_{\mathrm{in}}) \right) \exp\left(- \frac{U_{\mathrm{ext}} A_{\mathrm{ext}}}{\dot{m}_{\mathrm{fl}} c_{\mathrm{fl}}} \right). \tag{10}$$

A main assumption made above is that the temperature change of the thermally connected component, e.g. adsorbent, is small during the residence time of a fluid particle. The temperature of the adsorbent changes due to two effects: 1) the heat transfer from or to the heat transfer fluid and 2) the adsorption or desorption process. However, both effects are coupled and the heat transfer usually dominates in packed-bed adsorbers considered in this work (Aristov, 2013). For adsorption chillers, the heat transfer to the adsorbent is generally poor due to the porous adsorbent and the near-vacuum conditions. In contrast, the heat transfer fluid has a high heat capacity rate. For this reason, the adsorbent barely changes its temperature during the residence time of a fluid particle. To test this assumption, we define a characteristic number CN which can be derived from a dimensional analysis of Equation 4:

$$\mathrm{CN} = \frac{U_{\mathrm{ext}}}{v_{\mathrm{fl}} \rho_{\mathrm{fl}} c_{\mathrm{fl}}}. \tag{11}$$

The characteristic number CN relates the overall heat transfer to the heat capacity rate of the heat transfer fluid. A small characteristic number CN means that the overall heat transfer to the thermally connected component is low compared to the heat capacity rate of the fluid. Consequently, a small characteristic number CN supports the assumption of a small temperature change of the connected component for the residence time of the fluid particle. In Section 5, the validity of this assumption is tested for characteristic numbers CN typical in adsorption chillers.

To calculate the outlet temperature in Equation 10, the overall heat transfer value $U_{\mathrm{ext}}A_{\mathrm{ext}}$ is needed. The overall heat transfer value can be used as a parameter to calibrate the model to experimental data (van der Heijde et al., 2017). To account for the dependence of the heat transfer coefficient on the mass flow, we follow the approach of Lanzerath (2013) and decompose the overall heat transfer value ($U_{\mathrm{ext}}A_{\mathrm{ext}}$) into the flow-dependent external heat transfer value ($h_{\mathrm{ext}}A_{\mathrm{ext}}$) and the internal heat transfer value ($h_{\mathrm{int}}A_{\mathrm{int}}$) (cf. Equation 5). While the internal heat transfer value ($h_{\mathrm{int}}A_{\mathrm{int}}$) is used as calibration parameter of the model, the external heat transfer coefficient is calculated based on empirical correlations from literature. The correlations for the external heat transfer coefficient as well as the pressure drop are described in the supporting information A.1.

Equivalent fluid volume

The delay of the heat transfer due to the heat exchanger wall was neglected in the energy balance in Equation 4. However, the thermal mass of the heat exchanger wall needs to be accounted for. This thermal mass is important, since the heat exchanger wall of the adsorber is cycled between adsorption and desorption temperature. Consequently, the energy needed to change the temperature of the heat exchanger wall influences, e.g., the coefficient of performance.

To account for the thermal mass of the heat exchanger wall, we add an equivalent, ideally mixed fluid volume at the end of the heat exchanger model, which has the same thermal mass as the heat exchanger wall. The energy balance of the equivalent fluid volume reads:

$$V_{\mathrm{eq}} \rho_{\mathrm{fl}} \frac{\mathrm{d}h_{\mathrm{fl,out}}^{\mathrm{eq}}}{\mathrm{d}t} = \dot{m}_{\mathrm{fl}} \left(h_{\mathrm{fl,in}}^{\mathrm{eq}} - h_{\mathrm{fl,out}}^{\mathrm{eq}} \right), \tag{12}$$

where V_{eq} is the geometric volume of the fluid. This geometric volume is calculated from the thermal mass of the heat exchanger wall:

$$V_{\mathrm{eq}} = \frac{m_{\mathrm{wall}} c_{\mathrm{wall}}}{\rho_{\mathrm{fl}} c_{\mathrm{fl}}}, \tag{13}$$

where m_{wall} is the mass and c_{wall} is the specific heat capacity of the heat exchanger wall.

The position of the equivalent fluid volume at the end of the heat exchanger has an additional advantage for the numerical solution of the model: When the heat exchangers are connected to other system models, the equivalent fluid volume hydraulically separates the connected models and, thus, avoids systems of non-linear equations (van der Heijde et al., 2017).

2.2. Adsorber bed

The adsorber bed includes the adsorbent and the adsorbate. To model the adsorber bed, we use a lumped-parameter approach based on the work of Lanzerath et al. (2015). The lumped-parameter model assumes a homogenous temperature, loading, and pressure inside the adsorber bed.

2.2.1. Differential balances

The adsorber bed model contains two differential balances, which describe the time-dependent changes of the differential states, namely the loading w (mass balance):

$$m_{\mathrm{sor}} \frac{\mathrm{d}w}{\mathrm{d}t} = \dot{m}_{\mathrm{in/out}}, \tag{14}$$

and the temperature T (energy balance):

$$m_{\mathrm{sor}} (c_{\mathrm{sor}} + w c_{\mathrm{ad}}) \frac{\mathrm{d}T}{\mathrm{d}t} = \dot{m}_{\mathrm{in/out}} \left(h_{\mathrm{in/out}} - u_{\mathrm{ad}} \right) + \dot{Q}, \tag{15}$$

where m_{sor} and c_{sor} denote the mass of the adsorbent and the specific heat capacity of the adsorbent, respectively. The specific heat capacity of the adsorbate c_{ad} is approximated by the specific heat capacity of the liquid phase (Chakraborty et al., 2007).

In Equation 15, the flows on the right hand side are derived from the connected models and the sub-models: The incoming specific enthalpy h_{in} and the heat flow $\dot{Q}$ are determined by the connected models. To calculate the incoming or leaving mass flow ($\dot{m}_{\mathrm{in/out}}$), the kinetics model is employed, while the internal energy of the adsorbate u_{ad} is derived from the equilibrium model. Finally, the leaving specific enthalpy h_{out} is calculated by the fluid properties of the adsorptive as a function of the current temperature T of the adsorber bed and the pressure of the

adsorbate p_{ad}, which is also calculated by the equilibrium model.

2.2.2. Equilibrium model

The task of the equilibrium model is to fully describe the state of the working pair, given two of three states (temperature, pressure, or loading). Within the adsorber-bed model, the equilibrium model delivers the pressure of the adsorbate p_{ad} and the internal energy of the adsorbate u_{ad} for the differential balances, and the equilibrium loading w_{eq} for the kinetics model. In this work, the equilibrium is described by the model of Dubinin (Dubinin, 1967). We use a characteristic curve $A(W)$ of the working pair silica gel 123 / water, which was experimentally determined by Schawe (1999), since both investigated adsorption chillers employ this working pair. However, any other equilibrium model can also be implemented in the adsorber-bed model.

For given temperature (T) and loading (w) from the differential balances (Equations (14) and (15)), the pressure of the adsorbate p_{ad} can be derived by calculating the filled pore volume $W(w,T)$ and using the inverse of the characteristic curve ($W^{-1}(A) = A(W)$):

$$p_{ad} = p_{sat}(T)\ \exp\frac{-A(W)}{RT}. \tag{16}$$

The specific internal energy of the adsorbate u_{ad} is also calculated by the equilibrium model as:

$$u_{ad} = h_{ad} - \frac{p_{ad}}{\rho_{ad}}, \tag{17}$$

where the specific enthalpy of the adsorbate h_{ad} results from the model of Dubinin and the density of the adsorbate ρ_{ad} is approximated by the density of the liquid phase.

To determine the equilibrium loading w_{eq}, the temperature of the adsorber bed T and the pressure at the fluid port p are used to calculate the adsorption potential $A(T,p)$. The adsorption potential allows to calculate the filled pore volume using the characteristic curve $W(A)$ and delivers the equilibrium loading w_{eq}:

$$w_{eq} = W\ \rho_{ad}. \tag{18}$$

2.2.3. Kinetics model

The kinetics model delivers the mass flow $\dot{m}_{in/out}$ adsorbed or desorbed by the adsorber bed to the differential balances. For this purpose, the adsorption rate in the mass balance (Equation 14) is described by the linear driving force (LDF) approach and determines the mass flow $\dot{m}_{in/out}$ as function of the equilibrium loading w_{eq} and the current loading w:

$$\dot{m}_{in/out} = m_{sor}\frac{15D_{eff}}{r^2_{particle}}\left(w_{eq} - w\right), \tag{19}$$

where D_{eff} is the effective diffusion coefficient and $r_{particle}$ is the particle radius. The effective diffusion coefficient D_{eff} summarizes all transport resistances between the vapor phase and the adsorbate, and is used as a calibration parameter of the model in the following.

2.3. VLE volume

To describe the refrigerant in the evaporator and the condenser, we use a lumped-parameter model of a VLE volume, which is also based on the work of Lanzerath et al. (2015). In the VLE model, the refrigerant is assumed to be always in the two-phase region. Furthermore, the liquid phase and the vapor phase are always in thermodynamic equilibrium.

The VLE model contains two differential balances, which describe the time-dependent changes of the differential states, namely the density ρ (mass balance):

$$V\frac{\mathrm{d}\rho}{\mathrm{d}t} = \dot{m}_{in} - \dot{m}_{out}, \tag{20}$$

and the temperature T (energy balance):

$$V\left(u + \rho\left(\frac{\partial u}{\partial \rho}\right)_T\right)\frac{\mathrm{d}\rho}{\mathrm{d}t} + V\rho c_v\frac{\mathrm{d}T}{\mathrm{d}t} = \dot{m}_{in}h_{in} - \dot{m}_{out}h_{out} + \dot{Q}, \tag{21}$$

where V is the geometric volume of the evaporator or the condenser, and c_v is the specific isochoric heat capacity of the refrigerant.

The partial derivative of the internal energy u with respect to the density ρ can be formulated as (Tummescheit, 2002):

$$\left(\frac{\partial u}{\partial \rho}\right)_T = \frac{1}{\rho^2}\left(-p + T\frac{\mathrm{d}p}{\mathrm{d}T}\right). \tag{22}$$

As the refrigerant is in the two-phase region, the derivative of the pressure with respect to the temperature results from the Clausius-Clapeyron equation:

$$\frac{\mathrm{d}p}{\mathrm{d}T} = \frac{\Delta h_v}{T\left(v_v - v_{liq}\right)}, \tag{23}$$

where Δh_v is the specific enthalpy of vaporization, v_v is the specific volume of the vapor phase, and v_{liq} is the specific volume of the liquid phase.

The entering and leaving mass flows ($\dot{m}_{in}$ and $\dot{m}_{out}$), the incoming specific enthalpy h_{in}, and the heat flow $\dot{Q}$ result from the connected models. The leaving specific enthalpy h_{out} results either from the specific enthalpy of the saturated vapor at the vapor port or from the specific enthalpy of the boiling liquid at the liquid port.

3. Comparison of the plug-flow-based and the discretized adsorption chiller model

To evaluate the plug-flow-based adsorption chiller model, we calibrate and validate the model with experimental data from a lab-scale one-bed adsorption chiller (Lanzerath, 2013; Lanzerath et al., 2015). The considered adsorption chiller test-stand and the corresponding parametrization of the models are described in the supporting information D.

The calibration and validation method employed here is described in the supporting information C. Lanzerath et al. (2015) also used the same method for the validation of a 1-d, lumped-parameter model (discretized model), which serves as a reference model in the following. Thereby, we can directly compare the plug-flow-based model to an experimentally validated state-of-the-art model, regarding both, accuracy and computational efficiency (simulation time). The accuracy of the models is characterized by the average coefficient of variation of the entire adsorption chiller ($\overline{CV}$): The ($\overline{CV}$) is defined as the average root-mean-square deviation (RMSD) between simulated and measured heat flows of the adsorption chiller weighted by their corresponding average heat flows (see supporting information C.1 for detailed definition).

As the discretized model trades-off accuracy and computational efficiency depending on the discretization resolution, we consider two cases for the discretized model:

1. A fine discretization of 40 cells in the adsorber, and 10 cells in the evaporator and the condenser. Lanzerath (2013) determined this fine discretization resolution empirically since a finer discretization had no further significant impact on the simulation results. Therefore, the fine discretization serves as the reference model to achieve high accuracy.
2. A coarse discretization of 5 cells in the adsorber, and 2 cells in the evaporator and the condenser. This coarse discretization achieves a similar computational efficiency as the plug-flow-based model. Therefore, the coarse discretization serves as the reference model to achieve high computational efficiency.

The discretization resolution is discussed in detail in the supporting

information B.

3.1. Calibration

The adsorption chiller model is calibrated by the two-step calibration approach (cf. supporting information C.2) for the calibration cycle used by Lanzerath (2013):

1. evaporator inlet temperature of 10 °C,
2. condenser and adsorption inlet temperature of 35 °C,
3. desorption inlet temperature of 90 °C, and
4. adsorption and desorption time of 900 s.

The estimated calibration parameters of the plug-flow-based adsorption chiller model are shown in Table 1 and compared to those of the discretized model (Lanzerath, 2013).

The estimated heat transfer value of the evaporator is practically identical for both models (deviation of 4 %). In contrast, the estimated heat transfer coefficient of the condenser differs most between the two models with 37 %. However, the heat transfer coefficient of the condenser barely impacts the simulation results since the internal heat transfer in the condenser is not limiting the process (cf. resistance analysis by Bau (2018)). Thus, its exact value is hard to estimate, as the optimum is very flat. Even if using the heat transfer value estimated by Lanzerath (2013) in the plug-flow-based model (3174 W/K instead of 2005 W/K), the coefficient of variation of the adsorption chiller only changes less than 1 %. In the adsorber, large deviations are observed for the heat transfer value and the effective diffusion coefficient. These deviations can be explained by the linear dependence of both parameters, as also mentioned by Lanzerath (2013): A higher diffusion coefficient compensates a lower heat transfer coefficient and vice versa. Thus, Lanzerath (2013) gives a range for both parameters with $(h_{\mathrm{int}}A_{\mathrm{int}})^{\mathrm{A}} = 250\mathrm{W/K}...480\mathrm{W/K}$ and $D_{\mathrm{eff}} = 1.3\times10^{-10}\mathrm{m^2/s}...2.7\times10^{-10}\mathrm{m^2/s}$, which includes both parameter values identified for the plug-flow-based model (cf. Table 1). Nevertheless, using the parameters of Lanzerath (2013) in the plug-flow-based model would worsen the coefficient of variation of the adsorption chiller by 16%. Thus, a separate calibration of the plug-flow-based model is important to achieve good model accuracy.

All estimated heat transfer coefficients are higher for the plug-flow-based model than for the discretized model (Table 1). We expect that this systematic difference is due to two reasons: 1) The plug-flow-based model assumes a constant temperature at the process-side of the heat exchanger for each entering fluid particle (cf. Section 2.1). This assumption leads to a higher driving force for heat transfer, since the temperature at the process side is changing in reality due to the heat transfer. To compensate this higher driving force, the estimated heat transfer coefficient is lower for the plug-flow-based model. 2) The discretized model employs an upwind discretization scheme. The upwind scheme uses the leaving temperature of each fluid cell to calculate the heat transfer. Thereby, the driving force is underestimated for a finite discretization, since the driving force of the entering fluid is higher than that of the leaving fluid in each cell. To compensate the lower driving force, the estimated heat transfer coefficient is higher for the discretized model.

Table 1
Estimated calibration parameters for the plug-flow-based and the discretized adsorption chiller model: 3 internal heat transfer values of evaporator $(h_{\mathrm{int}}A_{\mathrm{int}})^{\mathrm{E}}$, condenser $(h_{\mathrm{int}}A_{\mathrm{int}})^{\mathrm{C}}$, and adsorber $(h_{\mathrm{int}}A_{\mathrm{int}})^{\mathrm{A}}$ and effective diffusion coefficient D_{eff} of the mass transfer model, cf. Section 2.2.3

	Discretized model	Plug-flow-based model	Deviation
$(\mathbf{h_{int}A_{int}})^{\mathrm{E}}$	176 W/K	169 W/K	-4 %
$(\mathbf{h_{int}A_{int}})^{\mathrm{C}}$	3174 W/K	2005 W/K	-37 %
$(\mathbf{h_{int}A_{int}})^{\mathrm{A}}$	331 W/K	257 W/K	-22 %
$\mathbf{D_{eff}}$	$1.8\times10^{-10}\mathrm{m^2/s}$	$2.41\times10^{-10}\mathrm{m^2/s}$	34 %

Figure 1 shows the excellent agreement between the experimental data and the simulations of both models (plug-flow-based and finely discretized) for the calibration cycle. The y-axis of the heat flow of the adsorber is cut off at 2.5 kW since the exchange of hot and cold heat transfer fluid inside the heat exchanger causes a very high peak, that is one order of magnitude higher than the heat flows shown.

The plug-flow-based model leads to practically identical results as the finely discretized model. The $\overline{\mathrm{CV}}$-value of the plug-flow-based model is even slightly lower (13.5 %) than the $\overline{\mathrm{CV}}$-value of the finely discretized model (13.6 %). Thus, both models provide the same accuracy. However, the simulation of the plug-flow-based model is three times faster than the simulation of the finely discretized model. The coarsely discretized model achieves a similar simulation time as the plug-flow-based model, but the $\overline{\mathrm{CV}}$-value increases by 71 % to 23.1 %.

Still, the models show deviations from the experiment: The peak of the heat flow of the evaporator at the beginning of the cycle (Figure 1 (a) at 100-200 s) is slightly overestimated by the models. Furthermore, the model slightly underestimates the heat flows of the adsorber in the adsorption phase (Figure 1 (b) at 100-400 s) and the desorption phase (Figure 1 (d) at 1000-1200 s). As all deviations arise in both models, we expect that this model inaccuracy does not result from the proposed plug-flow-based approach. Potential reasons for the deviations are discussed in the supporting information F.

3.2. Validation

To validate the plug-flow-based adsorption chiller model, we fix the calibration parameters determined for the calibration cycle (Section 3.1) and evaluate the model accuracy for changed operating conditions (inlet temperature and adsorption/desorption time Table 2).

For the seven validation cycles, Figure 2 compares the plug-flow-based model to the discretized model regarding both, accuracy and computational efficiency.

Regarding the accuracy, the plug-flow-based and the finely discretized model are equivalent, with even a slight preference for the plug-flow-based model (Figure 2 (a)): The $\overline{\mathrm{CV}}$-values are almost equal for the calibration cycle (C) and for the validation cycles V4 and V7. For the validation cycles V1, V2 and V6, the $\overline{\mathrm{CV}}$-values of the plug-flow-based model are even lower by 25 %, 11 % and 27 %, respectively. Only in the validation cycles V3 and V5, the plug-flow-based model has higher $\overline{\mathrm{CV}}$-values by 7 % and 11 %, respectively.

The average coefficient of variation ($\overline{\mathrm{CV}}$) of the plug-flow-based model is between 9.3 % and 30.4 % for all validation cycles. Lanzerath (2013) also stated a similar range of $\overline{\mathrm{CV}}$-values between 12.6 % and 27.4 % for his finely discretized model. Furthermore, Lanzerath (2013) showed that even for a $\overline{\mathrm{CV}}$-value of 27.4 % the simulated and the measured heat flows showed good qualitative agreement and the performance indicators coefficient of performance COP and specific cooling power SCP were almost predicted within the measurement uncertainties. Thus, the similar $\overline{\mathrm{CV}}$-range of the plug-flow-based model indicates that the calibrated model is also able to predict different operating points than the calibration cycle.

Regarding computational efficiency, the plug-flow-based model significantly outperforms the finely discretized model, as the simulation time is reduced by 65 %-70 % in all cycles (Figure 2 (b)). To achieve the computational efficiency of the plug-flow-based model, the resolution of the discretized model has to be reduced by 75 % (coarsely discretized model). However, the coarsely discretized model has much worse accuracy, increasing the $\overline{\mathrm{CV}}$-values between 13 % in the validation cycle V5 and 130 % in the validation cycle V1 compared to the plug-flow-based model.

To emphasize the quality of the plug-flow based model, Figure 3 compares the predicted performance indicators of the adsorption chiller

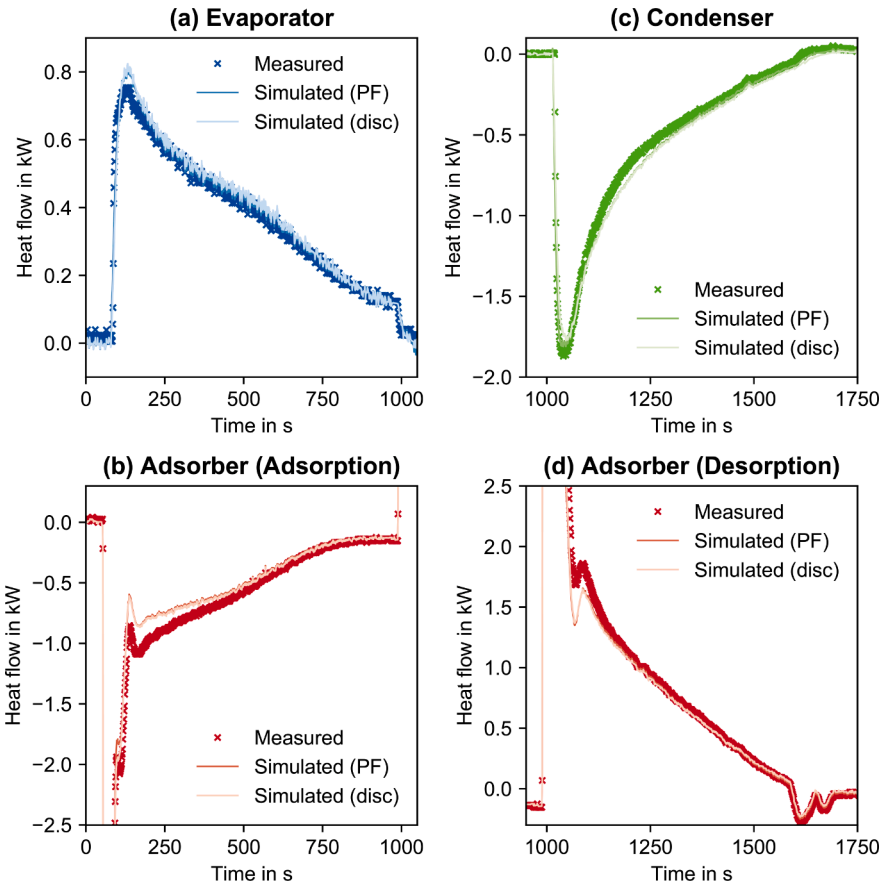

Fig. 1. Measured and simulated heat flows of the lab-scale one-bed adsorption chiller (Lanzerath, 2013) in the calibration cycle. The simulated heat flows of both models, plug-flow-based (PF) and discretized (disc), are practically identical and, therefore, hard to distinguish.

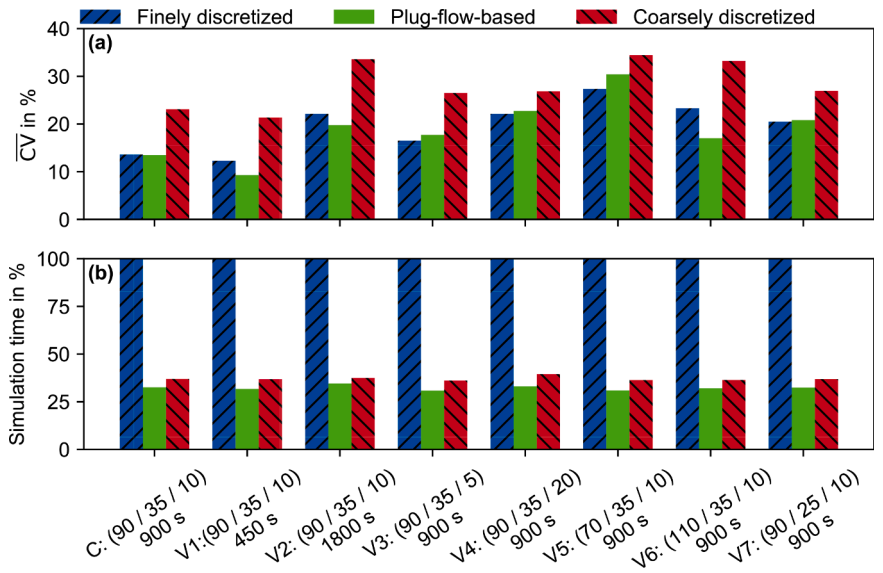

Fig. 2. Comparison of the plug-flow-based and the discretized model of the lab-scale adsorption chiller for the calibration cycle (C) and the validation cycles (V1-V7) (Table 2). (a) Average coefficient of variation $\overline{CV}$ (cf. supporting information C). (b) Relative simulation time referred to the finely discretized model.

(coefficient of performance COP and specific cooling power SCP) to those of the accurate, finely discretized model and the measured values.

The predicted performance indicators are mostly within the measurement uncertainties. The largest deviation from the measured values for both performance indicators (COP and SCP) can be observed in the validation cycle V4, where the simulated values are slightly outside the measurement uncertainty. In the validation cycle V4, the plug-flow-based model is closer to the measured values than the finely discretized model: The deviation from the measured COP is 16 % for the finely discretized model and 13 % for the plug-flow-based model. The deviation from the measured SCP is 12 % for the finely discretized model and 10 % for the plug-flow-based model.

Table 2
Variation of the operating conditions (inlet temperatures and adsorption/desorption time) for the validation cycles of the lab-scale, one-bed adsorption chiller (Lanzerath, 2013). The varied condition compared to the calibration cycle (first line) is printed in bold.

Desorption inlet temperature in °C	Condenser / adsorption inlet temperature in °C	Evaporator inlet temperature in °C	Adsorption / desorption time in s
90	35	10	900
90	35	10	**450**
90	35	10	**1800**
90	35	**5**	900
90	35	**20**	900
70	35	10	900
110	35	10	900
90	**25**	10	900

While both models under- and overestimated the specific cooling power of the adsorption chiller, the COP is overestimated systematically. This systematic overestimation of the COP results from the underestimation of the heat flow of the heating circuit (Figure 1) due to the additional thermal masses of the test stand not considered in the model (cf. discussion in supporting information F). To improve the accuracy of the model further, the additional thermal masses can be added to the model in future work. Note that the same systematic overestimation of the COP arises in both models (Figure 3) and thus, is not a specific drawback of the proposed plug-flow-based approach.

The results show that the plug-flow-based adsorption chiller model has practically the same accuracy as the finely discretized model but significantly improves the computational efficiency by more than 65 %. The improved computational efficiency results from the drastic reduction of differential equations since the discretized model needs to solve the energy balance in each fluid and wall cell. Therefore, the finely discretized model has 88 % more differential equations (126 differential equations) than the plug-flow-based model (15 differential equations).

4. Model validation for a commercial two-bed adsorption chiller

In this section we used experimental data of the commercial adsorption chiller *Invensor LTC 30 e plus* (Invensor GmbH, 2020) and applied the calibration and validation method from supporting information C. The configuration of the commercial adsorption chiller is described in the supporting information E.

4.1. Calibration

The calibration step estimates the calibration parameters of the model, namely the internal heat transfer values of the heat exchangers and the effective diffusion coefficient, cf. supporting information C.2. As calibration cycle, we use the nominal operating point defined by the manufacturer (temperature triple 85 / 27 / 18):

1. heating temperature of 85 °C,
2. heat-rejection temperature of 27 °C and
3. cooling temperature of 18 °C.

The manufacturer provided time-resolved measurement data within a cooperation project, for which a non-disclosure agreement applied. Therefore, time-resolved data shown in the following is normalized.

Figure 4 shows the excellent agreement between the measured and the simulated heat flows for the calibration cycle.

The $\overline{CV}$-value of the model in the calibration cycle is 13 %, which is even slightly lower than for the lab-scale adsorption chiller in Section 3.1 (13.5 %). Nevertheless, the model shows deviations from the experimental data: (1) The model slightly overestimates the peak of the heat flow of the cooling circuit at the beginning of the cycle (Figure 4 (a) at normalized time between 0.1-0.2). (2) The model slightly underestimates the heat flow of the heating circuit (Figure 4 (b) at normalized time between 0.1-0.2) and the heat flow of the heat rejection circuit (Figure 4 (c) at normalized time between 0.2-0.4). Both deviations also arose for the lab-scale one-bed adsorption chiller. For a discussion of these deviations, the reader is therefore referred to supporting information F.

4.2. Validation

Next, we validate the model by varying the operating conditions of the adsorption chiller and evaluating the accuracy of the calibrated model with fixed calibration parameters (Table 3).

Note that, the validation cycles differ from those in Table 2:

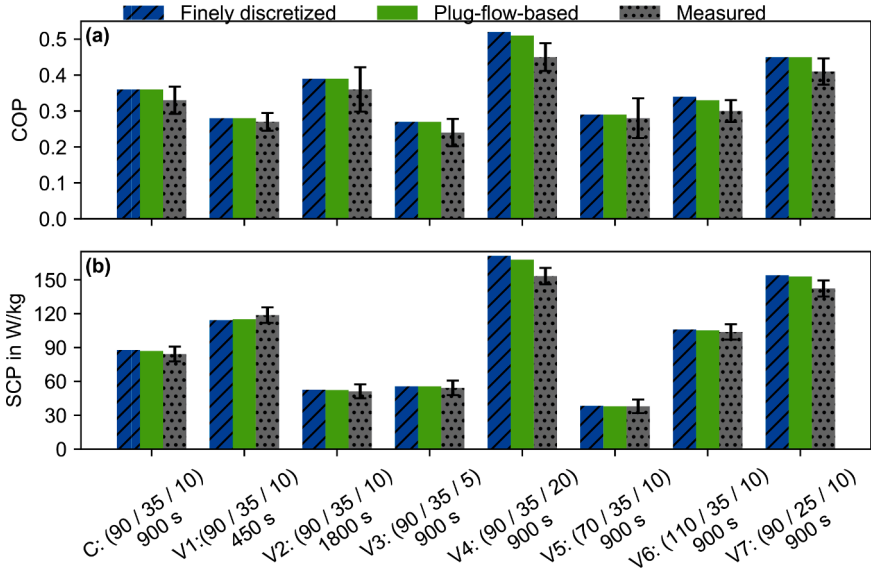

Fig. 3. Prediction of the performance indicators of both models and comparison to the measured values: (a) coefficient of performance COP and (b) specific cooling power SCP. The measurement uncertainties are indicated by black bars.

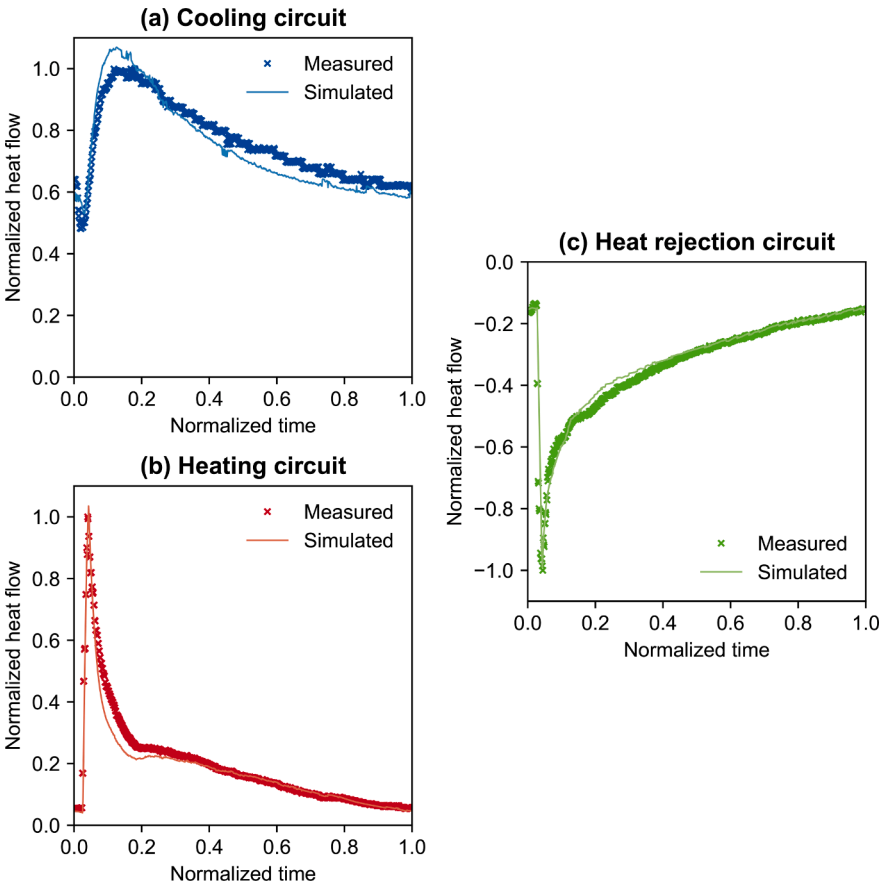

Fig. 4. Measured and simulated heat flows of the commercial two-bed adsorption chiller *Invensor LTC 30 e plus* (Invensor GmbH, 2020) in the calibration cycle. The axes are normalized by their maximal value.

1. The cycle time is not manually varied, but determined by an internal control algorithm. Therefore, the cycle time is different in each validation cycle.
2. More than one operating condition is varied simultaneously compared to the calibration cycle.
3. The volume flows in the hydraulic circuits are also varied. The nominal volume flows are given in the data-sheet of the adsorption chiller (Invensor GmbH, 2020): 6300 l/h in the heating circuit, 11400 l/h in the heat-rejection circuit, and 6600 l/h in the cooling circuit.

Figure 5 shows the accuracy of the calibrated model for the validation cycles.

The average coefficient of variation $\overline{CV}$ for all validation cycles is between 13.1 % and 20 % (Figure 5 (a)), which corresponds to a maximal relative increase of the $\overline{CV}$ by 54% compared to the calibration cycle (13 %). This increase of the $\overline{CV}$ in the validation cycles is even lower than for the models of the lab-scale adsorption chiller in Section 3.2 (increase of up to 100 %). The absolute values of the $\overline{CV}$ are also in the same range as for the model of the lab-scale adsorption chiller (Section 3.2).

Furthermore, the coefficient of performance COP and the average cooling power are also predicted very accurately: The deviation between the measured and the simulated value ranges from 2.9 % to 11.5 % for the COP (Figure 5 (b)) and from 1.2 % to 6.5 % for the average cooling power (Figure 5 (c)). These deviations from the measured values are also even lower than for the models of the lab-scale adsorption chiller (Section 3.2). The results show that the plug-flow-based model can also describe the commercial two-bed adsorption chiller with high accuracy.

While the average cooling power of the adsorption chiller is both, under- and overestimated by the model, the COP is overestimated systematically. This systematic overestimation also arose for the lab-scale one-bed adsorption chiller. For a discussion of this overestimation the reader is referred to Section 3.2.

Overall, the proposed model shows a good agreement for the considered commercial adsorption chiller. Thus, the plug-flow-based modeling approach proves to be applicable for different types of adsorption chillers.

5. Validity of the plug-flow-based model

In this section, we further test the validity range of the plug-flow-based modeling approach. For this purpose, we focus on the adsorber as the key component of the adsorption chiller. We consider an adsorber with an ideal evaporator and condenser (constant pressure boundaries, cf. supporting information B). The adsorber is parametrized according to the lab-scale adsorption chiller investigated in Section 3 and employs its calibration cycle.

As discussed in Section 2.1, the proposed plug-flow-based heat exchanger model assumes that the temperature change of the thermally connected component is small during the residence time of a fluid particle. This assumption can be tested by varying the characteristic number (Equation 11) that is the ratio of overall heat transfer to heat capacity rate. Therefore, we analyze the simulated heat flows of the plug-flow-based adsorber and of the finely discretized adsorber as function of the characteristic number CN (Figure 6). The deviation between both models is referred to as the error of the plug-flow-based model in the following. To quantify the error of the plug-flow-based model, we use the normalized coefficient of variation (cf. supporting information C.1) of the adsorber (A) (CV^A): the CV between the plug-

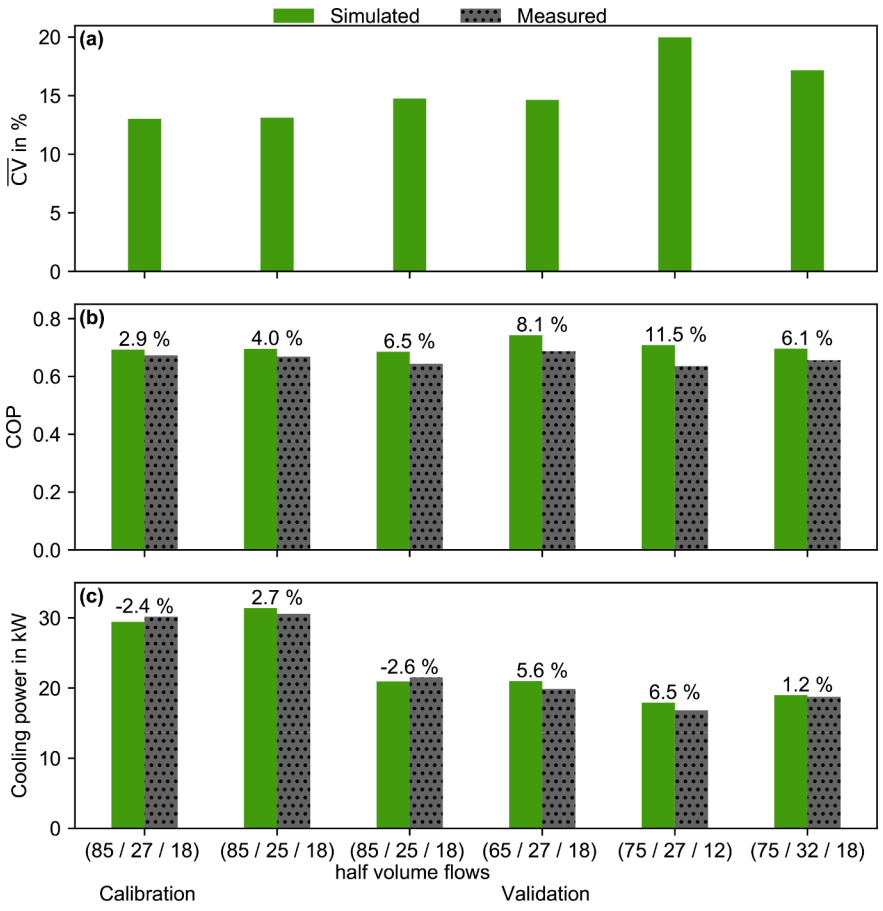

Fig. 5. Validation of the plug-flow-based model of the *Invensor LTC 30 e plus* adsorption chiller (Invensor GmbH, 2020) for all measured cycles (Table 3). (a) Average coefficient of variation $\overline{CV}$ (cf. supporting information C). Comparison between the measured and the simulated values of (b) the coefficient of performance COP and (c) the average cooling power. The deviations between simulated and measured values are given above the bars.

Table 3
Variation of the operating conditions (inlet temperatures and volume flows) for the validation cycles of the *Invensor LTC 30 e plus* adsorption chiller (Invensor GmbH, 2020). The varied conditions compared to the calibration cycle (first line) are printed in bold.

Heating circuit inlet temperature in °C	Heat rejection circuit inlet temperature in °C	Cooling circuit inlet temperature in °C	Volume flows
85	27	18	nominal
85	**25**	18	nominal
85	**25**	18	**halved**
65	27	18	nominal
75	27	**12**	nominal
75	**32**	18	nominal

flow-based and the discretized adsorber model (CV^{A}_{model}) is normalized by the CV between the measurement and the simulation of the adsorber (CV^{A}_{meas}) in the calibration cycle (Section 3.1). The error of the plug-flow-based model is shown for three thermal mass ratios of adsorbent ($(mc)_{sor}$) to heat transfer fluid ($(mc)_{fl}$). The thermal mass ratio of 0.56 corresponds to the lab-scale one-bed adsorption chiller (Section 3). The discretized adsorber was discretized into 100 cells to ensure that the simulation results are independent of the discretization (see supporting information B).

As expected, the error of the plug-flow-based adsorber increases with an increasing characteristic number CN (Figure 6), since the model assumption of a small temperature change of the connected adsorber bed during the residence time of a fluid particle (cf. Section 2.1) no longer holds. For the same reason, the error of the plug-flow-based model decreases if the thermal mass of the adsorbent ($(mc)_{sor}$) increases compared to the heat transfer fluid ($(mc)_{fl}$) since thermal inertia

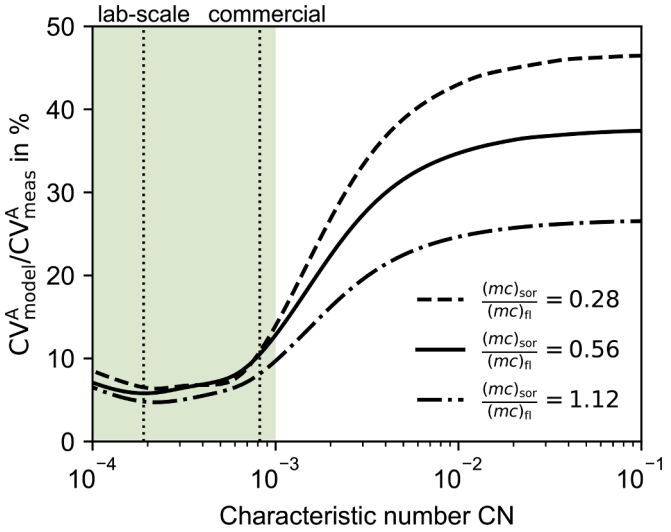

Fig. 6. Error of the plug-flow-based model as a function of the characteristic number CN (Equation 11). The characteristic numbers CN of the lab-scale adsorber (Section 3) and of the commercial adsorber (Section 4) are shown as vertical lines. The green shading indicates our recommended range for the use of the plug-flow-based model.

is increased and, thus, temperature changes even slower.

In all cases, the error of the plug-flow-based model is less than 50 % of the deviation between measurement and simulation. For small characteristic numbers CN below 1×10^{-3}, the error of the plug-flow-based model is less than 14 % and very similar for all three ratios of thermal masses. In contrast, the error increases strongly for characteristic numbers CN above 1×10^{-3}. Furthermore, the error also increases for small mass ratios more strongly. Therefore, we recommend the use of the plug-flow-based model for characteristic numbers CN between 1×10^{-4} and 1×10^{-3} (green shading in Figure 6). Outside this range of characteristic numbers CN, we recommend a case-specific analysis to decide whether the error of the plug-flow-based model is acceptable. However, we expect that most adsorption chillers will be covered by the recommended range, as shown for the lab-scale (Section 3) and the commercial (Section 4) adsorption chiller in this paper (Figure 6).

Note that for very small characteristic numbers CN (approximately below 2×10^{-4}), the error of the plug-flow-based model also slightly increases. The reason for this increase is that the thermal connection between the adsorber bed and the heat exchanger becomes very poor since the convective heat transfer is very small. Therefore, almost no heat is transferred to the adsorber bed and the model mainly describes the dynamics of the heat exchanger wall. However, the thermal inertia of the heat exchanger wall is approximated by an equivalent fluid volume (Equation 13). This approximation assumes that the dynamics of the wall are negligible compared to the dynamics of the adsorber bed (cf. Section 2.1). This assumption no longer holds for very small characteristic numbers CN below 1×10^{-4}, since the adsorber bed practically does not participate in the heating and cooling process. However, we believe that very small characteristic numbers CN below 1×10^{-4} are irrelevant for technical adsorption chillers, as the adsorber bed is almost thermally isolated from the heat exchanger leading to an inefficient process. Thus, the proposed, plug-flow-based modeling approach is well suited for technically relevant conditions in adsorption chillers.

6. Summary

The spatial discretization of heat exchangers often leads to computationally expensive models of adsorption chillers. Here, we proposed an alternative modeling approach for the heat exchangers to improve computational efficiency while ensuring high accuracy. The proposed approach avoids the discretization of the heat exchanger models by applying operator splitting to the partial differential equation of the fluid transport leading to a plug-flow-based model.

The proposed model proved to be as accurate as a finely discretized model of a lab-scale one-bed adsorption chiller: The average coefficient of variation $\overline{CV}$, which characterizes the deviation from experimental heat flows, was similar for both models or even lower by up to 26 % for the plug-flow-based model. The plug-flow-based model was able to predict the main performance indicators of the adsorption chiller (coefficient of performance COP and specific cooling power SCP) more accurately than the discretized model: The deviation from measured COP was below 12 % for the plug-flow-based model, while the deviation was up to 16 % for the discretized model. The deviation from measured SCP was below 10 % for the plug-flow-based model, while the deviation was up to 12 % for the discretized model. At the same time, the computational efficiency of the plug-flow-based model was significantly higher by up to 70 % compared to the discretized model.

The applicability of the proposed model was also demonstrated for a commercial two-bed adsorption chiller. Here, the plug-flow-based model retained the same good accuracy as for the lab-scale one-bed adsorption chiller.

Finally, the validity of the proposed plug-flow-based model was tested by varying a characteristic number CN that relates the overall heat transfer to the heat capacity rate of the fluid. We found that the plug-flow-based model is well suited in the range of characteristic numbers CN between 1×10^{-4} and 1×10^{-3}. Outside this range of characteristic numbers CN, we recommend a case-specific analysis to test the model validity.

Overall, the proposed plug-flow-based modeling approach provides an accurate and computationally efficient alternative to the discretization of heat exchangers of adsorption chiller models. The high computational efficiency makes the model well suited for addressing complex design and control optimizations of full-scale adsorption chiller systems.

Declaration of Competing Interest

The authors declare that they have no known competing financial interests or personal relationships that could have appeared to influence the work reported in this paper.

Acknowledgements

We gratefully acknowledge the financial support from the German Federal Ministry for Education and Research (BMBF) in the founding initiative “KMU innovativ” via the project Sorb Zero (01LY1827B).

Supplementary material

Supplementary material associated with this article can be found, in the online version, at10.1016/j.ijrefrig.2022.04.015

References

Abd-Elhady, M.M., Hamed, A.M., 2020. Effect of fin design parameters on the performance of a two-bed adsorption chiller. International Journal of Refrigeration 113, 164–173. https://doi.org/10.1016/j.ijrefrig.2020.01.006.

Alam, K.C.A., Akahira, A., Hamamoto, Y., Akisawa, A., Kashiwagi, T., 2004. A four-bed mass recovery adsorption refrigeration cycle driven by low temperature waste/renewable heat source. Renewable Energy 29 (9), 1461–1475. https://doi.org/10.1016/j.renene.2004.01.011.

Aristov, Y.I., 2013. Experimental and numerical study of adsorptive chiller dynamics: Loose grains configuration. Applied Thermal Engineering 61 (2), 841–847. https://doi.org/10.1016/j.applthermaleng.2013.04.051.

Batchelor, G.K., 2000. An Introduction to Fluid Dynamics. Cambridge University Press, Cambridge. https://doi.org/10.1017/CBO9780511800955.

Bau, U., 2018. From Dynamic Simulation to Optimal Designand Control of Adsorption Energy Systems. RWTH Aachen University. Phd thesis.

Bau, U., Baumgärtner, N., Seiler, J., Lanzerath, F., Kirches, C., Bardow, A., 2019. Optimal operation of adsorption chillers: First implementation and experimental evaluation of a nonlinear model-predictive-control strategy. Applied Thermal Engineering 149, 1503–1521. https://doi.org/10.1016/j.applthermaleng.2018.07.078.

Boelman, E.C., Saha, B.B., Kashiwagi, T., 1995. Experimental investigation of a silica gel-water adsorption refrigeration cycle - the influence of operating conditions on cooling output and COP. ASHRAE Transactions 101 (Pt 2), 358–366.Proceedings of the 1995 ASHRAE Annual Meeting ; Conference date: 24-06-1995 Through 28-06-1995

Buonomano, A., Calise, F., Palombo, A., 2018. Solar heating and cooling systems by absorption and adsorption chillers driven by stationary and concentrating photovoltaic/thermal solar collectors: Modelling and simulation. Renewable and Sustainable Energy Reviews 82, 1874–1908. https://doi.org/10.1016/j.rser.2017.10.059.

Calabrese, L., Bruzzaniti, P., Palamara, D., Freni, A., Proverbio, E., 2020. New sapo-34-speek composite coatings for adsorption heat pumps: Adsorption performance and thermodynamic analysis. Energy 203. https://doi.org/10.1016/j.energy.2020.117814.

Chakraborty, A., Saha, B.B., Koyama, S., Ng, K.C., 2007. Specific heat capacity of a single component adsorbent-adsorbate system. Applied Physics Letters 90 (17). https://doi.org/10.1063/1.2731438.

Critoph, R.E., 1999. Forced convection adsorption cycle with packed bed heat regeneration: Cycle á adsorption á convection forcée avec régénération thermique du lit fixe. International Journal of Refrigeration 22 (1), 38–46. https://doi.org/10.1016/S0140-7007(97)00036-4.

Dalibard, A., 2017. Advanced control strategies of solar driven adsorption chillers. Technische Universitåt Berlin. Phd thesis.

Dawoud, B., Vedder, U., Amer, E.H., Dunne, S., 2007. Non-isothermal adsorption kinetics of water vapour into a consolidated zeolite layer. International Journal of Heat and Mass Transfer 50 (11), 2190–2199. https://doi.org/10.1016/j.ijheatmasstransfer.2006.10.052.

Denzinger, C., Berkemeier, G., Winter, O., Worsham, M., Labrador, C., Willard, K., Altaher, A., Schuleter, J., Ciric, A., Choi, J.-K., 2021. Toward sustainable refrigeration systems: Life cycle assessment of a bench-scale solar-thermal

adsorption refrigerator. International Journal of Refrigeration 121, 105–113. https://doi.org/10.1016/j.ijrefrig.2020.09.022.
Douss, N., Meunier, F.E., Sun, L.M., 1988. Predictive model and experimental results for a two-adsorber solid adsorption heat pump. Industrial & Engineering Chemistry Research 27 (2), 310–316. https://doi.org/10.1021/ie00074a017.
Dubinin, M.M., 1967. Adsorption in micropores. Journal of Colloid and Interface Science 23 (4), 487–499. https://doi.org/10.1016/0021-9797(67)90195-6.
Gibelhaus, A., Tangkrachang, T., Bau, U., Seiler, J., Bardow, A., 2019. Integrated design and control of full sorption chiller systems. Energy 185, 409–422. https://doi.org/10.1016/j.energy.2019.06.169.
Gluesenkamp, K.R., Frazzica, A., Velte, A., Metcalf, S., Yang, Z., Rouhani, M., Blackman, C., Qu, M., Laurenz, E., Rivero-Pacho, A., Hinmers, S., Critoph, R., Bahrami, M., Füldner, G., Hallin, I., 2020. Experimentally measured thermal masses of adsorption heat exchangers. Energies 13 (5), 1150. https://doi.org/10.3390/en13051150.
Graf, S., Eibel, S., Lanzerath, F., Bardow, A., 2020. Validated performance prediction of adsorption chillers: Bridging the gap from gram-scale experiments to full-scale chillers. Energy Technology 8 (5). https://doi.org/10.1002/ente.201901130.
Graf, S., Redder, F., Bau, U., de Lange, M., Kapteijn, F., Bardow, A., 2019. Toward optimal metal–organic frameworks for adsorption chillers: Insights from the scale-up of MIL-101(cr) and NH 2 -MIL-125. Energy Technology 8 (1), 1900617. https://doi.org/10.1002/ente.201900617.
Gråber, M., Kirches, C., Bock, H.G., Schlöder, J.P., Tegethoff, W., Köhler, J., 2011. Determining the optimum cyclic operation of adsorption chillers by a direct method for periodic optimal control. International Journal of Refrigeration 34 (4), 902–913. https://doi.org/10.1016/j.ijrefrig.2010.12.021.
van der Heijde, B., Fuchs, M., Ribas Tugores, C., Schweiger, G., Sartor, K., Basciotti, D., Müller, D., Nytsch-Geusen, C., Wetter, M., Helsen, L., 2017. Dynamic equation-based thermo-hydraulic pipe model for district heating and cooling systems. Energy Conversion and Management 151, 158–169. https://doi.org/10.1016/j.enconman.2017.08.072.
Invensor GmbH, 2020. Adsorption Chiller InvenSor LTC 30 e plus. https://www.invensor.com/en/products/invensor-ltc-30-e-plus/.
Karagiorgas, M., Meunier, F., 1987. The dynamics of a solid-adsorption heat pump connected with outside heat sources of finite capacity. Heat Recovery Systems and CHP 7 (3), 285–299. https://doi.org/10.1016/0890-4332(87)90141-4.
Krzywanski, J., Grabowska, K., Herman, F., Pyrka, P., Sosnowski, M., Prauzner, T., Nowak, W., 2017. Optimization of a three-bed adsorption chiller by genetic algorithms and neural networks. Energy Conversion and Management 153, 313–322. https://doi.org/10.1016/j.enconman.2017.09.069.
Lanzerath, F., 2013. Modellgestützte Entwicklung von Adsorptionswärmepumpen (in German). RWTH Aachen University. Phd thesis.
Lanzerath, F., Bau, U., Seiler, J., Bardow, A., 2015. Optimal design of adsorption chillers based on a validated dynamic object-oriented model. Science and Technology for the Built Environment 21 (3), 248–257. https://doi.org/10.1080/10789669.2014.990337.
Lazrak, A., Boudehenn, F., Bonnot, S., Fraisse, G., Leconte, A., Papillon, P., Souyri, B., 2016. Development of a dynamic artificial neural network model of an absorption chiller and its experimental validation. Renewable Energy 86, 1009–1022. https://doi.org/10.1016/j.renene.2015.09.023.
MacNamara, S., Strang, G., 2016. Operator Splitting. Springer International Publishing. https://doi.org/10.1007/978-3-319-41589-5_3.
Mahdavikhah, M., Niazmand, H., 2013. Effects of plate finned heat exchanger parameters on the adsorption chiller performance. Applied Thermal Engineering 50 (1), 939–949. https://doi.org/10.1016/j.applthermaleng.2012.08.033.
Meunier, F., Neveu, P., Castaing-Lasvignottes, J., 1998. Equivalent carnot cycles for sorption refrigeration: Cycles de carnot équivalents pour la production de froid par sorption. International Journal of Refrigeration 21 (6), 472–489. https://doi.org/10.1016/S0140-7007(97)00084-4.
Modelica Association, 2017. Modelica ®- A Unified Object-Oriented Language for Systems Modeling, Language Specification Version 3.4. https://www.modelica.org/documents/ModelicaSpec34.pdf.
Mohammed, R.H., Mesalhy, O., Elsayed, M.L., Chow, L.C., 2019. Assessment of numerical models in the evaluation of adsorption cooling system performance. International Journal of Refrigeration 99, 166–175. https://doi.org/10.1016/j.ijrefrig.2018.12.017.
Muttakin, M., Islam, M.A., Malik, K.S., Pahwa, D., Saha, B.B., 2020. Study on optimized adsorption chiller employing various heat and mass recovery schemes. International Journal of Refrigeration. https://doi.org/10.1016/j.ijrefrig.2020.12.032.
Nienborg, B., Dalibard, A., Schnabel, L., Eicker, U., 2017. Approaches for the optimized control of solar thermally driven cooling systems. Applied Energy 185, 732–744. https://doi.org/10.1016/j.apenergy.2016.10.106.
Oppelt, T., Urbaneck, T., Gross, U., Platzer, B., 2016. Dynamic thermo-hydraulic model of district cooling networks. Applied Thermal Engineering 102, 336–345. https://doi.org/10.1016/j.applthermaleng.2016.03.168.
Palomba, V., Ferraro, M., Frazzica, A., Vasta, S., Sergi, F., Antonucci, V., 2018. Experimental and numerical analysis of a sofc-chp system with adsorption and hybrid chillers for telecommunication applications. Applied Energy 216, 620–633. https://doi.org/10.1016/j.apenergy.2018.02.063.
Pesaran, A., Lee, H., Hwang, Y., Radermacher, R., Chun, H.-H., 2016. Review article: Numerical simulation of adsorption heat pumps. Energy 100, 310–320. https://doi.org/10.1016/j.energy.2016.01.103.
Radu, A.I., Defraeye, T., Ruch, P., Carmeliet, J., Derome, D., 2017. Insights from modeling dynamics of water sorption in spherical particles for adsorption heat pumps. International Journal of Heat and Mass Transfer 105, 326–337. https://doi.org/10.1016/j.ijheatmasstransfer.2016.09.079.
Roetzel, W., Luo, X., Chen, D., 2020. Design and Operation of Heat Exchangers and their Networks. Elsevier Inc. https://doi.org/10.1016/b978-0-12-817894-2.00007-8
Sah, R.P., Choudhury, B., Das, R.K., Sur, A., 2017. An overview of modelling techniques employed for performance simulation of low-grade heat operated adsorption cooling systems. Renewable and Sustainable Energy Reviews 74, 364–376. https://doi.org/10.1016/j.rser.2017.02.062.
Saha, B.B., Boelman, E.C., Kashiwagi, T., 1995. Computer simulation of a silica gel-water adsorption refrigeration cycle - the influence of operating conditions on cooling output and COP. ASHRAE Transactions 101 (Pt 2), 348–357.Proceedings of the 1995 ASHRAE Annual Meeting ; Conference date: 24-06-1995 Through 28-06-1995
Sawant, P., Bürger, A., Doan, M.D., Felsmann, C., Pfafferott, J., 2020. Development and experimental evaluation of grey-box models of a microscale polygeneration system for application in optimal control. Energy and Buildings 215. https://doi.org/10.1016/j.enbuild.2019.109725.
Schawe, D., 1999. Theoretical and experimental investigations of an adsorption heat pump with heat transfer between two adsorbers. University of Stuttgart. Phd thesis.
Schicktanz, M., Núñez, T., 2009. Modelling of an adsorption chiller for dynamic system simulation. International Journal of Refrigeration 32 (4), 588–595. https://doi.org/10.1016/j.ijrefrig.2009.02.011.
Sha, A.A., Baiju, V., 2021. Thermodynamic analysis and performance evaluation of activated carbon-ethanol two-bed solar adsorption cooling system. International Journal of Refrigeration 123, 81–90. https://doi.org/10.1016/j.ijrefrig.2020.12.006.
Sharafian, A., Bahrami, M., 2015. Critical analysis of thermodynamic cycle modeling of adsorption cooling systems for light-duty vehicle air conditioning applications. Renewable and Sustainable Energy Reviews 48, 857–869. https://doi.org/10.1016/j.rser.2015.04.055.
Teng, W.S., Leong, K.C., Chakraborty, A., 2016. Revisiting adsorption cooling cycle from mathematical modelling to system development. Renewable and Sustainable Energy Reviews 63, 315–332. https://doi.org/10.1016/j.rser.2016.05.059.
Tso, C.Y., Chao, C.Y.H., Fu, S.C., 2012. Performance analysis of a waste heat driven activated carbon based composite adsorbent - water adsorption chiller using simulation model. International Journal of Heat and Mass Transfer 55 (25-26), 7596–7610. https://doi.org/10.1016/j.ijheatmasstransfer.2012.07.064.
Tummescheit, H., 2002. Design and Implementation of Object-Oriented Model Libraries using Modelica. Lund University. Phd thesis.
Wang, X., Chua, H.T., 2007. Two bed silica gel-water adsorption chillers: An effectual lumped parameter model. International Journal of Refrigeration 30 (8), 1417–1426. https://doi.org/10.1016/j.ijrefrig.2007.03.010.
Wu, J.Y., Wang, R.Z., Xu, Y.X., 2000. Dynamic simulation and experiments of a heat regenerative adsorption heat pump. Energy Conversion and Management 41 (10), 1007–1018. https://doi.org/10.1016/S0196-8904(99)00161-2.
Yaïci, W., Entchev, E., 2019. Coupled unsteady computational fluid dynamics with heat and mass transfer analysis of a solar/heat-powered adsorption cooling system for use in buildings. International Journal of Heat and Mass Transfer 144, 118648. https://doi.org/10.1016/j.ijheatmasstransfer.2019.118648.
Yong, L., Sumathy, K., 2002. Review of mathematical investigation on the closed adsorption heat pump and cooling systems. Renewable and Sustainable Energy Reviews 6 (4), 305–338. https://doi.org/10.1016/s1364-0321(02)00010-2.